Composites Part C: Open Access 12 (2023) 100414

Contents lists available at ScienceDirect

Composites Part C: Open Access

journal homepage: www.elsevier.com/locate/composites-part-c-open-access

Performance evaluation analysis of Ti-6Al-4V foam fan blades in aircraft engines: A numerical study

Mertol Tüfekci

Department of Mechanical Engineering, Imperial College London, South Kensington Campus, London, SW7 2AZ, UK

ARTICLE INFO

Keywords:
Fan blades
Metallic foam
Ti-6Al-4V
Mori–Tanaka homogenisation
Finite element method

ABSTRACT

In the aerospace industry, the structures are subjected to significant loads and extreme conditions whilst being required to be lightweight and resilient. Metallic foams seem to meet these criteria. However, their usage in the aerospace applications are not as common as one would expect. To explore a potential application of foams, this study evaluates the performance of the foams of Ti-6Al-4V, a conventional material/alloy for aircraft engine fan blade applications performing numerical simulations. First, the mechanical properties of the Ti-6Al-4V alloy are calculated using the Mori–Tanaka mean-field homogenisation and finite element (FE) methods employing representative volume elements (RVE). Using those calculated material properties and the computer-aided design (CAD) model of a representative aircraft engine fan blade, the FE models are built. In these numerical models, the material properties and the rotational speed with the static aero-loads are selected as variables, whilst boundary conditions remain consistent to ensure a systematic investigation. Stress analysis and the prestressed modal analyses of the blades are performed, and the results are presented to discuss the impact of the void volume fraction of the alloy foams. This study reveals the complex nature of the mechanics of fan blades when made of foams.

1. Introduction

Being able to fly is among the most significant achievements of engineering. However. this has not been easy. It is an extremely complicated task to design an efficient aircraft, especially their engines, which hinge on the precise balance of countless components, each subjected to certain and different requirements of performance, safety, and durability [1,2]. Among these components, aircraft engine fan blade is a crucial component used in the modern aviation industry. They are required to endure remarkable mechanical and thermal loads, all while operating at extreme velocities [3,4]. The rotational body forces are particularly challenging loads for the design process since they primarily root from the system's own mass and dimensions, and therefore, the impact of high-speed rotation is known to be quite significant on the mechanics of the rotating systems [5,6]. Their efficiency and reliability can significantly influence the overall operation and economic operation of an aircraft, thereby making them a focal point in improving the aircraft design and performance [7].

Engineers and researchers have spent significant efforts to optimise the design of these blades, aiming to improve their aerodynamic efficiency, minimise their weight, reduce the vibration amplitudes, and enhance their durability [8,9]. The principles of aerodynamics predominantly determine the geometry of these blades. The laws of fluid dynamics tend to limit their shape, size, and positioning within the engine. In time, the studies in aerodynamics have led to highly optimised blade designs, leaving little room for further improvement without disrupting the core mechanisms of flight and propulsion. This situation has resulted in the exterior geometry design of fan blades reaching a point of saturation, with diminishing returns on any substantial innovations in their shape or configuration. However, the structural behaviour is also a crucial part of the design process that impacts the efficiency of the blade's interactions with the surrounding air [3,10–13].

Consequently, the challenge of designing fan blades with improved performance has shifted towards material science. The selection of material used in manufacturing fan blades is as critical as their geometrical design. Indeed, material properties like strength, stiffness, weight, and thermal stability directly influence the performance, efficiency, and durability of the blades. Conventionally, titanium and aluminium alloys are used for fan blades due to their specific stiffnesses and specific strengths [4]. However, as mentioned earlier, the usage of these conventional materials led to a saturation of the design of fan blades. Thus, advanced materials are employed to create alternatives. Composite materials are among these advanced materials. The use of composites has become quite common in the aviation industry. GE uses composite fan blades in GE90 and GE9x, and so does Rolls-Royce in

E-mail address: m.tufekci17@imperial.ac.uk.

https://doi.org/10.1016/j.jcomc.2023.100414
Received 1 August 2023; Received in revised form 13 September 2023; Accepted 12 October 2023
Available online 20 October 2023
2666-6820/© 2023 The Author. Published by Elsevier B.V. This is an open access article under the CC BY-NC-ND license (http://creativecommons.org/licenses/by-nc-nd/4.0/).

UltraFan. However, their manufacturing and modelling processes are considerably more complicated [14,15]. Hence, the design of the fan blade also becomes a heavier task [16,17].

Foams are also included within advanced materials as they can achieve lightweight without compromising on the stiffness and strength [18,19]. Nevertheless, like composites, their modelling and manufacturing is a more complicated process compared to the traditional materials [18]. Whilst the manufacturing methods are not similar to the manufacturing techniques for composites, the modelling approaches are the same. It is possible to employ finite element (FE) analysis as well as mean-field homogenisation techniques like Mori–Tanaka to model foams and composites [4,20–22].

Even though composites have been used in fan blades, there is no industrial application of metallic or polymeric foams in fan blades [23–25]. Also, the number of studies focusing on the possible implementation of foams on fan blades is limited [26,27]. However, the usage of Ti-6Al-4V alloy foams for fan blades can be considered since Ti-6Al-4V alloy foam is a material that brings together the proven performance of titanium alloys with the structural benefits of foam materials. With their combination of strength, stiffness, and lightweight, these foams can provide the next step for fan blade design and manufacturing.

This study aims to fill the gap in the performance evaluation of fan blades made of Ti-6Al-4V alloy foams. Therefore, a detailed numerical investigation of aircraft engine fan blades made of Ti-6Al-4V alloy foams is presented in this research. The numerical analysis includes a FE method, and static stress and prestressed modal analyses are performed using this FE model, considering various volume fractions of the foam as well as various stages of loading. By employing the Mori–Tanaka mean-field homogenisation and FE method performing on representative volume elements (RVE) that have randomly positioned and sized spherical voids, the mechanical properties of the foam of Ti-6Al-4V alloy are computed. Using these material properties, a representative model of an aircraft engine fan blade is constructed for FE analysis. The results, in terms of the effects of different volume fractions of alloy foam and various levels of loading, are discussed. It is shown that materials can play an important part in the design and performance of aircraft engine fan blades. Considering the most common blade designs incorporate either full or hollow cross-sections, it can be stated that this study contributes to the literature by discussing the new idea of a rotor/fan blade that is made of foam, which is an alternative and very efficient way to achieve lightweight materials/structures. Thus, using foams can help achieve a new optimised *equilibrium* of engine components using advanced materials like foams and composites.

2. Modelling: Materials and materials' internal structures

This study relies on numerical modelling to explore the performance of Ti-6Al-4V alloy, with an elastic modulus of 110 GPa, Poisson's ratio of 0.31, and a density of 4600 $\mathrm{kg/m^3}$, and its foams with various volume fractions up to 0.5 as aircraft engine fan blade material.

The material Ti-6Al-4V is known to be isotropic. as well as the foam materials that have predominantly randomly sized and positioned spherical voids. Therefore, the resultant properties of the foams are expected to be quasi-isotropic since the effects of the voids should be similar in all directions [28–30]. However, in this study, instead of assuming isotropy, material modelling is performed taking anisotropy into account for the resultant foam. Therefore, the stiffness tensor for an anisotropic material has to be employed.

The stiffness tensor for anisotropic materials can be represented in terms of engineering constants in matrix form as:

$$\mathbb{C} = \begin{pmatrix} E_{11}(1-\nu_{23}\nu_{32}) & E_{22}\nu_{12} & E_{33}\nu_{13} & 0 & 0 & 0 \\ E_{22}\nu_{21} & E_{22}(1-\nu_{31}\nu_{13}) & E_{33}\nu_{23} & 0 & 0 & 0 \\ E_{33}\nu_{31} & E_{33}\nu_{32} & E_{33}(1-\nu_{12}\nu_{21}) & 0 & 0 & 0 \\ 0 & 0 & 0 & G_{12} & 0 & 0 \\ 0 & 0 & 0 & 0 & G_{23} & 0 \\ 0 & 0 & 0 & 0 & 0 & G_{31} \end{pmatrix} \tag{1}$$

In the stiffness tensor $\mathbb{C}$, E_{11}, E_{22}, E_{33} represent the Young's moduli along the principal material directions $1, 2, 3$, respectively. The Poisson's ratios, denoted by $\nu_{12}, \nu_{21}, \nu_{23}, \nu_{32}, \nu_{13}, \nu_{31}$, establish the relationship between strains in different directions, signifying how a material contracts or expands perpendicularly to the applied stress. Lastly, G_{12}, G_{23}, G_{31} are the shear moduli in their respective planes, indicating the material's resistance to shearing deformations.

First, the mechanical properties of the Ti-6Al-4V alloy foams are computed for various volume fractions (V_f) of the voids the foams contain. Material modelling is performed using two different techniques, namely Mori–Tanaka mean-field homogenisation and FE methods that use RVEs. Fig. 1 displays the internal structure of the Ti-6Al-4V alloy foams via the generated RVEs' computer models, which are later used for the FE evaluation of the RVEs.

2.1. Mori–Tanaka homogenisation method

As the first step of the material modelling, the Mori–Tanaka homogenisation method is employed to compute the elastic properties of the foam of the alloy Ti-6Al-4V. The Mori–Tanaka homogenisation method is known to work quite well up to volume fractions V_f of approximately 0.4, and therefore the value 0.5 is judged to be acceptably accurate and, more importantly, consistent for the overall framework of this study [31,32].

2.1.1. Mathematical background

The Mori–Tanaka method assumes a two-phase (can be extended to n-phases) composite. These phases are a matrix with properties denoted by subscript m, and inclusions with properties indicated with subscript i. The essential/fundamental step of the Mori–Tanaka mean-field homogenisation method is the calculation of the Eshelby tensor S, which describes the elastic fields of an ellipsoidal inclusion in an infinite homogeneous isotropic elastic continuum.

The stress and strain in the matrix, σ_m and ϵ_m, can be related using the stiffness tensor of the matrix $\mathbb{C}_m$ as follows:

$$\sigma_m = \mathbb{C}_m : \epsilon_m \tag{2}$$

Similarly, the same can be done for the inclusion, the relation is:

$$\sigma_i = \mathbb{C}_i : \epsilon_i \tag{3}$$

The total strain in the composite ϵ can be expressed as the volume average of the strains in the matrix and the inclusion, which is represented as:

$$\epsilon = (1 - V_f)\epsilon_m + V_f\epsilon_i \tag{4}$$

Here, V_f denotes the volume fraction of the inclusions. Furthermore, the strain in the inclusion ϵ_i can be related to the strain in the matrix ϵ_m and the stresses in the matrix and the inclusion by the Eshelby tensor S as:

$$\epsilon_i = \epsilon_m + S : (\sigma_m - \sigma_i) \tag{5}$$

This relation makes it possible to represent the actual inclusion by an equivalent/idealised inclusion that generates the same average strain in the composite. The differential form/scheme of the Mori–Tanaka method can then be written as:

$$d\epsilon = (1 - V_f)d\epsilon_m + V_f d\epsilon_i = \mathbb{S} : d\sigma \tag{6}$$

Here, $\mathbb{S}$ indicates the secant modulus of the composite and is inversely related to the overall stiffness tensor $\mathbb{C}$ of the composite as shown below:

$$\mathbb{S} = \mathbb{C}^{-1} \tag{7}$$

The secant modulus $\mathbb{S}$ can be solved iteratively from the differential form/scheme, so the computation of the overall stiffness $\mathbb{C}$ of the composite is achieved.

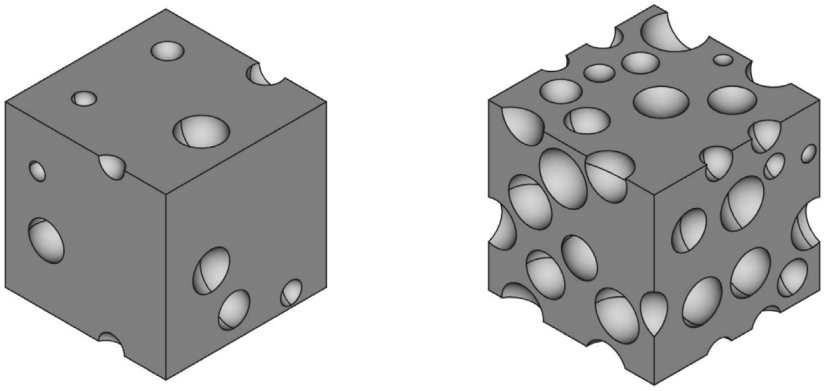

(a) $V_f = 0.1$. (b) $V_f = 0.3$.

Fig. 1. Representative structures of Ti-6Al-4V foams.

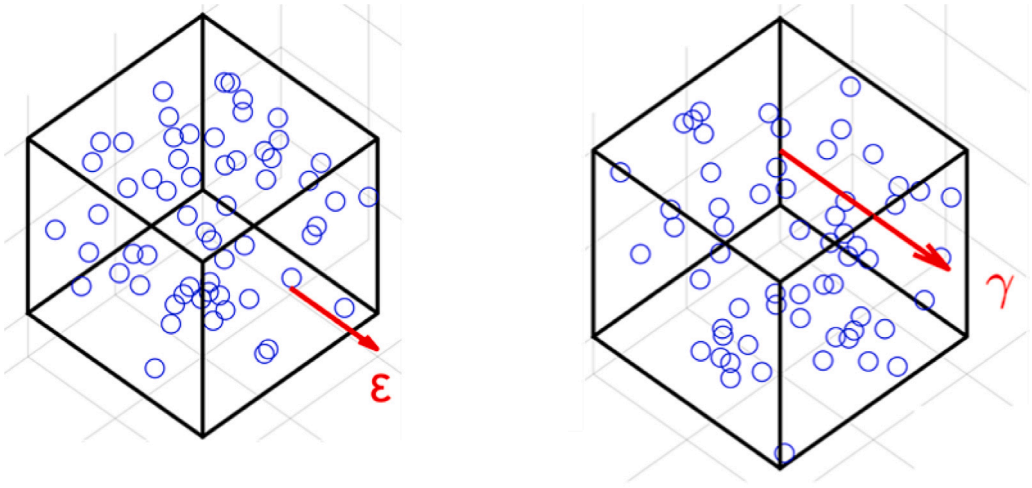

(a) Uniaxial tension. (b) Shear strain.

Fig. 2. A representative volume element under prescribed strain.

2.1.2. Physical background

The Mori–Tanaka method, as described above, is built on several physical assumptions. These mostly include the concepts of homogeneity, isotropy, and the principle of strain equivalence for the inclusion phase.

One of the basic assumptions is the matrix-inclusion representation. The composite material is seen as a combination of non-interacting inclusions dispersed in a continuous matrix. This assumption is one of the main reasons for the Mori–Tanaka method being more accurate in lover volume fractions of inclusions. The stress interaction between the inclusions becomes more significant as the distances between the inclusions are reduced. Obviously, higher volume fractions of inclusions lead to *tighter packing* of inclusions, and so the interparticular distances decrease, and the interactions of stress become more influential.

The matrix-inclusion representation assumes that the matrix material is effectively infinite, homogeneous, and isotropic, whilst the inclusions are treated as inserted ellipsoids. This simplifies the mathematical expressions as well as operations and permits an analytical solution. For the case of metallic foams in this study, the inclusions are considered as spherical voids with zero mass and stiffness.

The Eshelby tensor, which creates the basis of the Mori–Tanaka method, has a clear physical meaning. It represents the elastic fields of an ellipsoidal inclusion in an infinite, homogeneous, isotropic, elastic medium subjected to uniform remote stresses and strains.

The concept of equivalent inclusion is another important assumption of the Mori–Tanaka approach. The actual inclusion, which may be of complex shape and possess anisotropic and inhomogeneous properties, is represented with an equivalent ellipsoidal inclusion. The equivalent inclusion possesses the same average strain as the actual inclusion but is subjected to the same stress as the matrix. This simplification relieves the mathematical complexities significantly and is the reason behind the tractability of the Mori–Tanaka method.

The Mori–Tanaka method then employs a differential scheme, where the stresses and strains in the composite material are considered as the volume average of the stresses and strains in the matrix and inclusion. This scheme is designed to take into account the effects of both matrix and inclusions while maintaining the simplicity of a two-phase model.

The overall stiffness of the composite, the final output of the Mori–Tanaka method, can then be physically interpreted as the response of the composite material to applied stresses. The stiffer the composite, the less it deforms when subjected to a given stress.

It is important to remember that these simplifications and assumptions in the Mori–Tanaka method make it particularly suitable under certain conditions. For instance, as mentioned earlier, it performs better if the volume fraction of the inclusions is relatively low and the mechanical interactions of inclusions are not significant. Thus, the physical assumptions of the Mori–Tanaka method provide a practical framework for predicting the effective properties of composite materials.

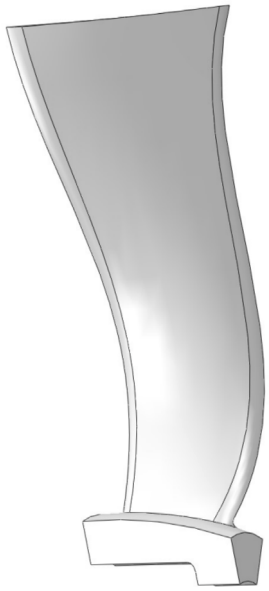

Fig. 3. Computer model of the representative fan blade structure.

2.2. Finite element approach

To start building the FE models, the geometries for the cubic RVEs containing stochastically distributed and sized spherical voids, are generated [15,33–36]. The void diameters are assumed to vary between 1 μm and 60 μm and the RVE parameter (edge length) is selected to be at least quintuple the greatest void diameter which makes the RVE actually *representative* of the foam [37–41]. After the generation of each RVE geometry, it is also checked and ensured that the void's volume fraction is acceptably near (±1%) the targeted volume fraction.

The FE models for the foam materials are constructed using the generated geometries of the RVEs. The geometries are meshed using a quadratic tetrahedral mesh, preparing them for simulation. This is followed by the introduction of periodic boundary conditions (PBC) and the imposition of loads in terms of uniaxial tensile and shear strain with a magnitude of 0.003. By doing so, both the micro-scale stresses and the effective mechanical properties are calculated. The prescribed strains are applied in each principal direction on the corresponding surfaces until all the engineering constants for an anisotropic material are calculated. The outcome of these calculations allows for a comprehensive understanding of the material's behaviour. To ensure the validity of these findings, simulations are performed for each set of material properties five times to confirm the robustness and repeatability of the results. Fig. 2 presents views of two sample RVEs generated for this research.

3. Modelling: Fan blade structure

To simulate the mechanical behaviour of the fan blade made of Ti-6Al-4V alloy foams, the computer-aided design (CAD) model of a representative fan blade is selected [4]. Geometrically and mechanically, this blade model is found to be accurate enough to represent an actual fan blade of a commercial civil aircraft engine that is made of Ti-6Al-4V alloy.

As shown in Fig. 3, the model integrates the blade and the disc as a single part. This removes the complexities of the contact nonlinearities from the system.

Following the preparation of the CAD model, the mesh generation is carried out on the three-dimensional geometry. Given the complex geometry of the blade structure, quadratic tetrahedral elements are used to accurately represent the structure. Thus approximately 50 000 elements and 80 000 nodes are generated.

The material properties, which are determined through the Mori–Tanaka mean-field homogenisation approach, are inserted into the model depending on the volume fraction of the voids in the foam being investigated. Even though the FE approach is the more robust one among the two material modelling methods employed, the results of Mori–Tanaka mean-field homogenisation is selected for the performance evaluation of the fan blade made of foam. The reasons behind this choice are, first, the Mori–Tanaka and FE approaches are expected

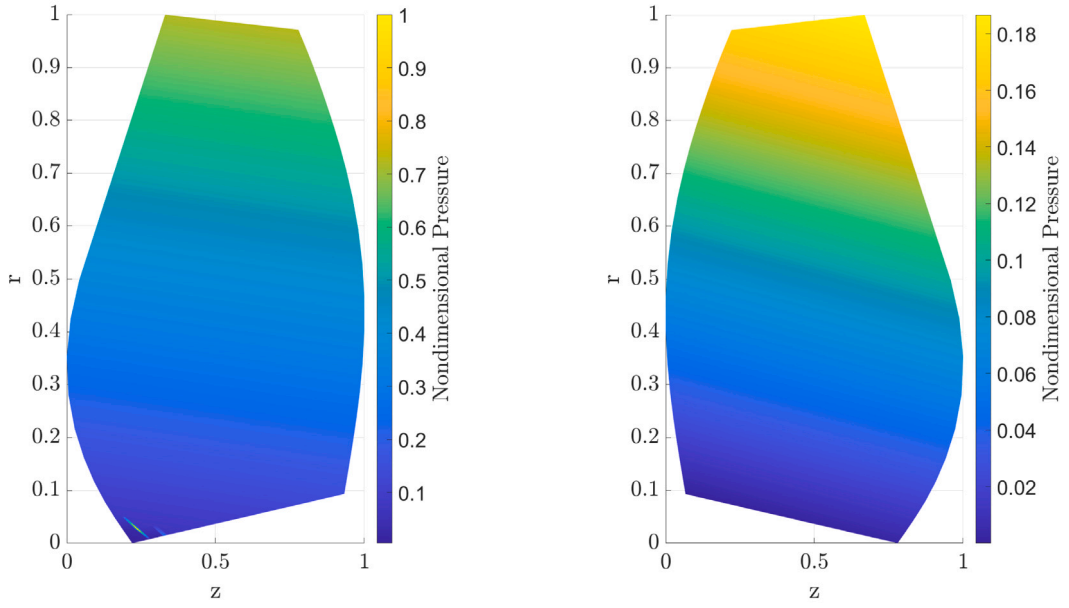

(a) Pressure side. (b) Suction side.

Fig. 4. Nondimensional pressure distribution for the pressure side (a) and suction side (b).

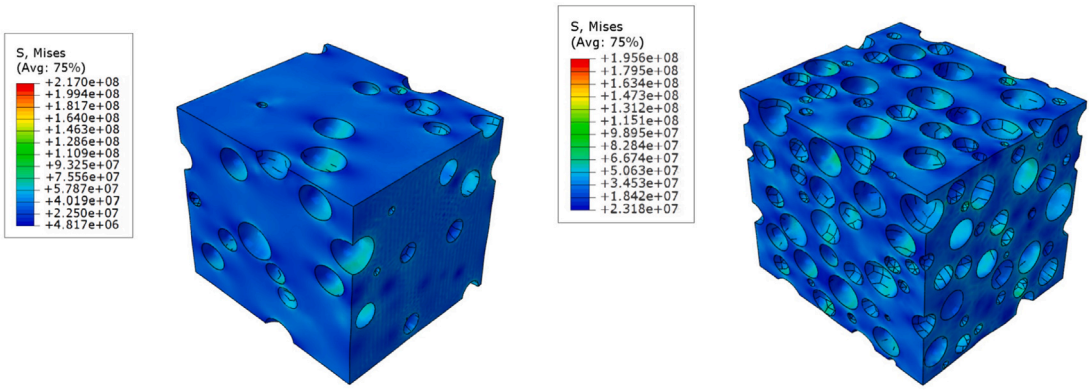

(a) $V_f = 0.1$. (b) $V_f = 0.3$.

Fig. 5. von Mises stress fields for different volume fractions computed with FE analysis (Stress in Pa).

Table 1
Engineering constants for different volume fractions calculated with Mori–Tanaka homogenisation (Units in Pa).

Engineering	Volume fractions V_f					
constants	0	0.1	0.2	0.3	0.4	0.5
E_{11}	1.10×10^{11}	9.00×10^{10}	7.33×10^{10}	5.92×10^{10}	4.71×10^{10}	3.66×10^{10}
E_{22}	1.10×10^{11}	9.00×10^{10}	7.33×10^{10}	5.92×10^{10}	4.71×10^{10}	3.66×10^{10}
E_{33}	1.10×10^{11}	9.00×10^{10}	7.33×10^{10}	5.92×10^{10}	4.71×10^{10}	3.66×10^{10}
G_{12}	4.20×10^{10}	3.47×10^{10}	2.85×10^{10}	2.31×10^{10}	1.85×10^{10}	1.45×10^{10}
G_{23}	4.20×10^{10}	3.47×10^{10}	2.85×10^{10}	2.31×10^{10}	1.85×10^{10}	1.45×10^{10}
G_{13}	4.20×10^{10}	3.47×10^{10}	2.85×10^{10}	2.31×10^{10}	1.85×10^{10}	1.45×10^{10}
ν_{12}	0.31	0.30	0.29	0.28	0.27	0.26
ν_{21}	0.31	0.30	0.29	0.28	0.27	0.26
ν_{13}	0.31	0.30	0.29	0.28	0.27	0.26
ν_{31}	0.31	0.30	0.29	0.28	0.27	0.26
ν_{23}	0.31	0.30	0.29	0.28	0.27	0.26
ν_{32}	0.31	0.30	0.29	0.28	0.27	0.26

to be in good agreement and, second and more importantly, considering the computational cost of the FE analysis for material modelling, this research aims to propose an *efficient* road-map for the development of fan blades made of foams.

The blade is fixed at the bottom surface of the disc, and cyclic symmetry is applied to the lateral surfaces of the disc. Finally, the loads are imposed to represent the operating conditions in steady-state, with the rotational speed set at 1000 rpm and a static aero-load acting on both surfaces of the blade. Thus, the representation of the operating conditions is achieved with some decent accuracy.

The pressure distribution on the fan blade is obtained by a comprehensive series of computational fluid dynamics simulations The resultant pressure data is visualised in Fig. 4 for both sides of the blade, namely the pressure side and the suction side. All pressure values are presented in a nondimensional form, normalised by dividing the entire dataset by the maximum pressure value in the pressure data. In Fig. 4 the pressure distributions on the pressure side and the suction side of the blade at the rotational speed of 1000 rpm (104 rad/s) are visualised. Here, z and r indicate spatial coordinates.

For further details about the model, the reader is encouraged to refer to the study by Tüfekci et al. [4].

Upon preparing the model, it is solved using Abaqus, a commercial FE software package, for the numerical analysis. Through static analysis, the stresses within the blade are calculated, as well as the displacements due to the deformation of the blade under the steady-state pressure loads.

For modal analysis, the prestressed model is put through to analysis to compute the natural frequencies and mode shapes of the blade.

The numerical investigation focuses on the impact of the loads depending on the rotational speed as well as the volume fraction of the foam on the stresses, displacements and natural frequencies, which can be used to gain an understanding of the stiffness, strength and inertial properties of the fan blade.

4. Results and discussion

4.1. Theoretical evaluation of the Ti-6Al-4V alloy foams

The first thing is to check if the foams are effectively isotropic or anisotropic by investigating the engineering constants in different directions. The engineering constants calculated by using the Mori–Tanaka mean-field homogenisation and the FE approaches given in Tables 1 and 2 are in very good agreement with each other and they strengthen the idea that the material's mechanical properties are quasi-isotropic alongside the reported cases in the literature [19,21,42–44]. The engineering constants indicate isotropy by $E_{11} \cong E_{22} \cong E_{33}$, $G_{12} \cong G_{23} \cong G_{13}$ and $\nu_{12} \cong \nu_{21} \cong \nu_{23} \cong \nu_{332} \cong \nu_{13} \cong \nu_{31}$ for the same volume fraction values of voids. This holds for every single value of void volume fraction. This results validate both methods against each other and legitimises the evaluation of material properties under the assumption of effective quasi-isotropic behaviour.

Fig. 5 visualises some representative stress analysis results acquired through FE calculations from two selected RVEs with $V_f = 0.1$ and $V_f = 0.3$. Here, the von Mises stress distribution is displayed considering the stress state is complicated and investigating a certain stress component might be misleading.

It can be clearly seen that there are stress concentrations around the voids' equators due to the existences of shear bands and stress triaxialities, which align with the previously reported and discussed results in the literature [45]. Moreover, the levels of stress drop with increasing void volume fractions. This is because of the definition of the loading of the RVE systems. The RVE is subjected to a constant uniaxial strain rather than forces and moments. Thus, the more compliant material

Table 2
Engineering constants for different volume fractions calculated with FE analysis (Units in Pa).

Engineering constants	Volume fractions V_f					
	0	0.1	0.2	0.3	0.4	0.5
E_{11}	1.10×10^{10}	8.95×10^{10}	7.26×10^{10}	5.70×10^{10}	4.46×10^{10}	3.68×10^{10}
E_{22}	1.10×10^{10}	8.93×10^{10}	7.23×10^{10}	5.69×10^{10}	4.51×10^{10}	3.70×10^{10}
E_{33}	1.10×10^{10}	8.92×10^{10}	7.25×10^{10}	5.71×10^{10}	4.45×10^{10}	3.70×10^{10}
G_{12}	4.20×10^{10}	3.44×10^{10}	2.79×10^{10}	2.22×10^{10}	1.77×10^{10}	1.50×10^{10}
G_{23}	4.20×10^{10}	3.45×10^{10}	2.80×10^{10}	2.21×10^{10}	1.74×10^{10}	1.47×10^{10}
G_{13}	4.20×10^{10}	3.45×10^{10}	2.80×10^{10}	2.22×10^{10}	1.76×10^{10}	1.46×10^{10}
ν_{12}	0.31	0.30	0.29	0.28	0.25	0.28
ν_{21}	0.31	0.30	0.29	0.28	0.25	0.27
ν_{13}	0.31	0.30	0.29	0.28	0.25	0.28
ν_{31}	0.31	0.30	0.29	0.28	0.25	0.27
ν_{23}	0.31	0.30	0.29	0.28	0.25	0.28
ν_{32}	0.31	0.30	0.29	0.28	0.25	0.28

Table 3
Comparison of relative modulus for Mori–Tanaka, FE, and values from Perez et al. [46].

Volume fraction (V_f)	Relative modulus (E/E_0) (Mori–Tanaka)	Relative modulus (E/E_0) (FE)	Relative modulus (E/E_0) (Experimental) [46]	Relative modulus (E/E_0) (FE) [46]
0	1.0000	0.1000	1.0000	1.0000
0.1	0.8182	0.8145	–	–
0.2	0.6664	0.6600	–	–
0.3	0.5382	0.5182	0.5667	0.5344
0.4	0.4282	0.4509	0.4460	0.5031
0.5	0.3332	0.3346	0.3984	0.3755

system is expected to display lower stress values which is the case here. The Mori–Tanaka and the FE analyses point out that the more voids present in a material the more is the stiffness reduced. Therefore, the drop of stress with growing void volume fraction is an expected result even though the stress concentrations and their interactions become more significant in foams with more voids.

The data presented in Table 3 provides a detailed comparison of the specific moduli (E/ρ) obtained using different methodologies. A noteworthy observation lies in the comparison of relative moduli (E/E_0) for varying volume fractions. In the case of a volume fraction of 0.3, the relative modulus obtained from the Mori–Tanaka method is 0.5382. This value shows only a 5.03% difference from the experimental value of 0.5667 from the literature, affirming the closeness of the method to experimental results. Likewise, when compared to the FE value of 0.5344 from the same study, the Mori–Tanaka result is 0.71% higher [46].

For a volume fraction of 0.4, the Mori–Tanaka method yields a relative modulus of 0.4282. The Mori–Tanaka value is 3.99% lower than the experimental value of 0.4460 and 14.89% lower than the FE value of 0.5031, both taken from the same study [46].

Continuing the trend at a volume fraction of 0.5, the Mori–Tanaka method predicts a relative modulus of 0.3332, which is 16.36% lower than the experimental value of 0.3984 and 11.26% lower than the FE value of 0.3755, both from the literature [46].

These minor variations can be attributed to multiple factors such as material heterogeneities, experimental conditions, or computational approximations and simplifications. However, the degree of correlation, especially in the context of specific and relative moduli, underlines the agreement between the Mori–Tanaka mean-field homogenisation method and the FE analyses. This strengthens the accuracy of the current computational models, reinforcing their reliability in predicting the mechanical behaviour of Ti-6Al-4V alloy foams. Moreover, these computational results are in very good agreement with experimental and FE findings presented in existing literature validating the conducted analyses [46].

Table 4 and Figs. 6 and 7 present the calculated mechanical properties of alloy foam using the Mori–Tanaka mean-field homogenisation and FE methods which are found to be in good agreement. These results outline the relationship between the volume fraction, V_f, density, ρ, Young's modulus, E, and specific modulus of the foams of Ti-6Al-4V alloy.

As expected, a clear pattern emerges from the data acquired from the Mori–Tanaka computations: as the volume fraction increases, there is a corresponding but not strictly proportional decrease in density, Young's modulus, and the specific modulus.

When the alloy without any voids is used, the highest Young's modulus of 1.10×10^{11} Pa and a specific modulus of 2.39×10^{7} m^2/s^2 are observed. Notably, the FE results are closely aligned with the Mori–Tanaka calculations, validating the homogenisation approach.

Then, the fall of stiffness and particular stiffness of the material declines. Consequently, at the highest volume fraction of voids, at 0.5, the foam displays the lowest values for these parameters: Young's modulus at 3.66×10^{10} Pa, and a specific modulus of 1.59×10^{7} m^2/s^2. The FE results corroborate this decrease, with slightly larger magnitudes.

This trend suggests that with an increase in the volume fraction of voids in the foam, the material becomes lighter (lower density), but its ability to withstand deformations (as represented by Young's modulus) and the ratio of stiffness to weight (specific modulus) decrease as well. This would be an expected outcome, as higher volume fractions typically correspond to more porosity in the foam, resulting in such reductions in stiffness. Moreover, the FE results generally agree with these trends but show some variances at certain volume fractions, highlighting the complexity of the foam's mechanical behaviour.

Even though these results give an idea of the physical understanding of the mechanics of foams, they do not provide enough to draw decisive conclusions. It is necessary to emphasise that these relationships are crucial but do not necessarily suffice to determine this alloy foam's appropriateness for specific applications. Especially considering that a significant part of the loads is rotational body forces, which depend on the mass of the fan blade, in other words, the density of the foam, these parameters obtained via Mori–Tanaka homogenisation and FE methods only hint towards a direction in the decision-making process of the material selection. Thus, balancing the required properties for the intended application against these trade-offs is essential in the design process and material selection.

4.2. Numerical modelling of the fan blade

4.2.1. Static analysis

To start evaluating the results of the FE model of the fan blade structure, first a mesh convergence analysis is carried out under the highest rotational speed and pressure. Fig. 8 shows that the stress increases less than 5% of the calculated stress when using 50 000 nodes which is the mesh that is used for this study. However, reducing the mesh size by

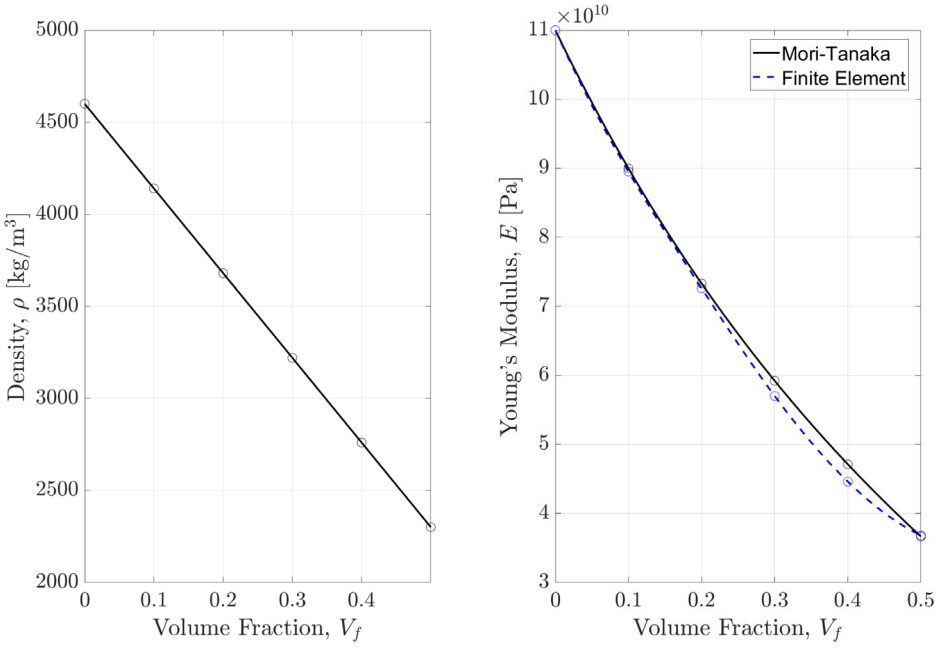

(a) Volume fraction (V_f) versus density (ρ). (b) Volume fraction (V_f) versus Young's modulus (E).

Fig. 6. The results from Mori–Tanaka homogenisation for the alloy foam.

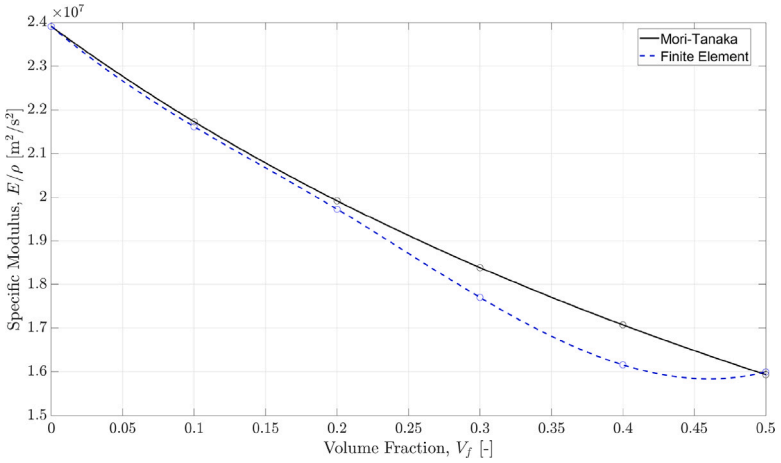

Fig. 7. Calculated specific modulus as a function of the volume fraction for the alloy foam.

Table 4
Mori–Tanaka and FE results for the alloy foam including Young's modulus and specific modulus.

Volume fraction (V_f)	Density (ρ) [kg/m^3]	Young's modulus (E) [Pa] (Mori–Tanaka)	Specific modulus (E/ρ) [m^2/s^2] (Mori–Tanaka)	Young's modulus (E) [Pa] (FE)	Specific modulus (E/ρ) [m^2/s^2] (FE)
0	4600	1.10×10^{11}	2.39×10^7	1.10×10^{11}	2.39×10^7
0.1	4140	9.00×10^{10}	2.17×10^7	8.95×10^{10}	2.16×10^7
0.2	3680	7.33×10^{10}	1.99×10^7	7.26×10^{10}	1.97×10^7
0.3	3220	5.92×10^{10}	1.84×10^7	5.70×10^{10}	1.77×10^7
0.4	2760	4.71×10^{10}	1.71×10^7	4.96×10^{10}	1.80×10^7
0.5	2300	3.66×10^{10}	1.59×10^7	3.68×10^{10}	1.60×10^7

half (increasing the node number up to 100 000) significantly increases the central processing unit (CPU) time. Therefore, the current mesh size is proven to be sufficiently efficient and accurate.

The results of the static analysis are presented in Table 5 and visually displayed in Figs. 9–12. The results include the maximum von Mises stress, the maximum principal stress, the maximum radial displacement and the maximum displacement magnitude calculated in the FE model of the fan blade.

The volume fraction, load, maximum von Mises stress, maximum principal stress, maximum displacement, and maximum radial displacement are the variables presented in this analysis.

First, focusing on the maximum von Mises stress (Fig. 9), it is seen that as the volume fraction of voids increases from 0 to 0.5, there is a general decrease in the maximum von Mises stress values for all the rotational speeds. For instance, at a rotational speed of 26 rad/s (250 rpm), the maximum von Mises stress decreases by approximately 41%

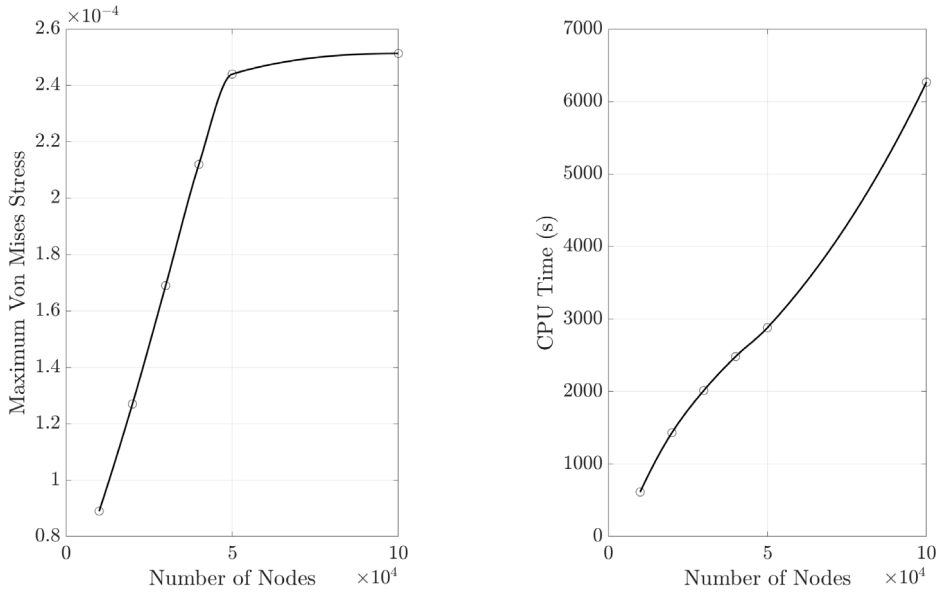

(a) Node numbers versus maximum von Mises stress. (b) Node numbers versus CPU time.

Fig. 8. Mesh convergence and CPU time plots for the FE analyses of the RVEs.

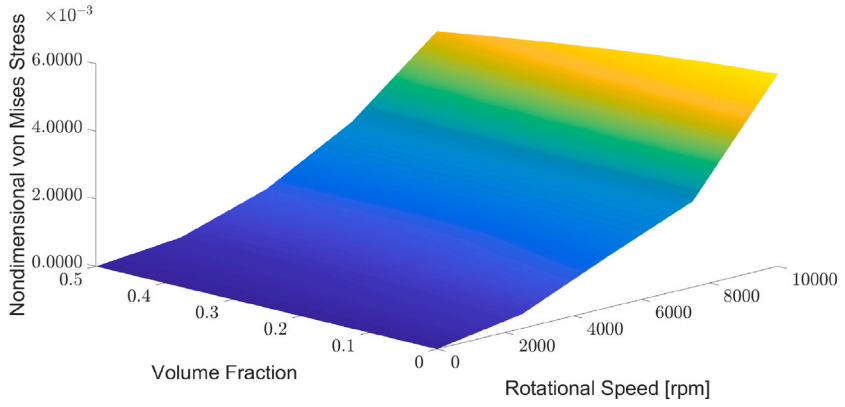

Fig. 9. Nondimensional von Mises stress versus rotational speed and volume fraction.

from 2.44×10^{-4} to 1.43×10^{-4}. Similarly, at 104 rad/s (1000 rpm), there is a drop of approximately 21% as V_f rises from 0 to 0.5. The maximum principal stress (Fig. 10) decreases with the increase in volume fraction across all rotational speeds following a similar trend. The correlation between the volume fraction of voids and the stresses observed in these simulations under static loading is primarily influenced by the rotational body forces. As the fan blade becomes lighter, the rotational body forces also drop. Of course, increasing volume fraction of voids also reduces the stiffness of the blade which also brings the stress down.

However, the maximum displacement magnitude and the maximum radial displacement do not strictly follow a monotonic pattern with increasing volume fractions of voids. The data in Figs. 11 and 12 reveal that at lower rotational speeds (26 rad/s and 52 rad/s), the maximum radial displacements and the maximum displacement magnitudes initially increase with the growing in volume fraction, reaching a peak. Then they start to fall. For higher rotational speeds (78 rad/s and 104 rad/s), the displacement values exhibit a decreasing trend with the increase in volume fraction. This is again due to the reduction of the blade's mass with increasing volume fractions. The radial displacements are predominately controlled by the rotational body forces. So the drop in radial displacement is a direct indication of the reduction of mass is more influential than the reduction of the stiffness when the volume fraction is increased. Also, even though the stiffness also drops, the decline of the displacement magnitudes suggests that the reduction of the rotational body forces has a more significant impact on the deformation of the blade than the pressure loads.

As expected, the growth of the rotational speed causes a rise in all the parameters tracked within the scope of the static simulations. This is due to the increasing centrifugal loads as well as the aero-pressure loads acting on the system. One thing to note here would be that the changes are more obvious for higher volume fractions compared to the changes in lower volume fractions of the voids in the foams.

The observations made from the results of the static analysis suggested that it is possible to reduce the stress in the blade and the deformation of the blade at the same time if the foam is tailored/tuned appropriately.

However, these results do not cover either the strength or the fatigue life, which are also critical for such components. Particularly, it is known that the voids in foams lead to stress concentrations which may lead to the reduction of strength and fatigue life.

Notably, it is observed that the results are seen aligned with the studies that proposed usage of foams as core materials for blades made designs using sandwich structures [26,27].

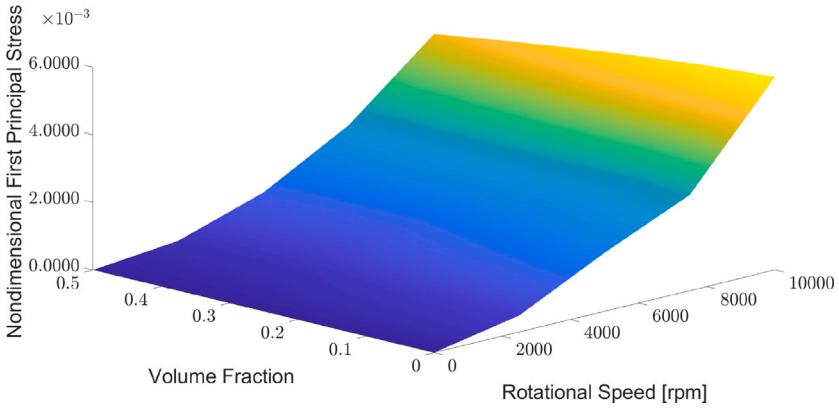

Fig. 10. Nondimensional first principal stress versus rotational speed and volume fraction.

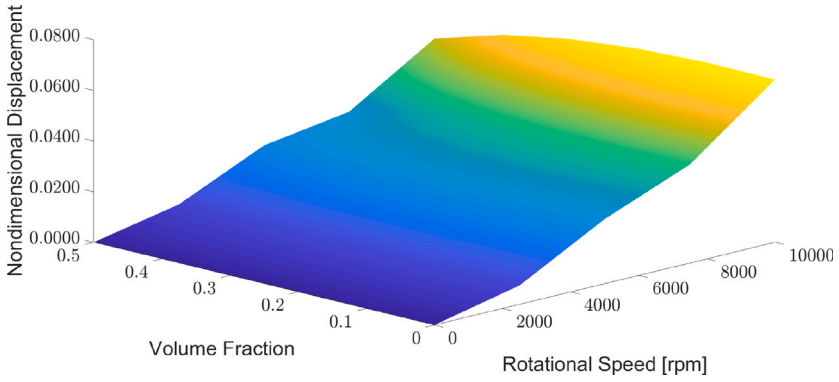

Fig. 11. Nondimensional displacement versus rotational speed and volume fraction.

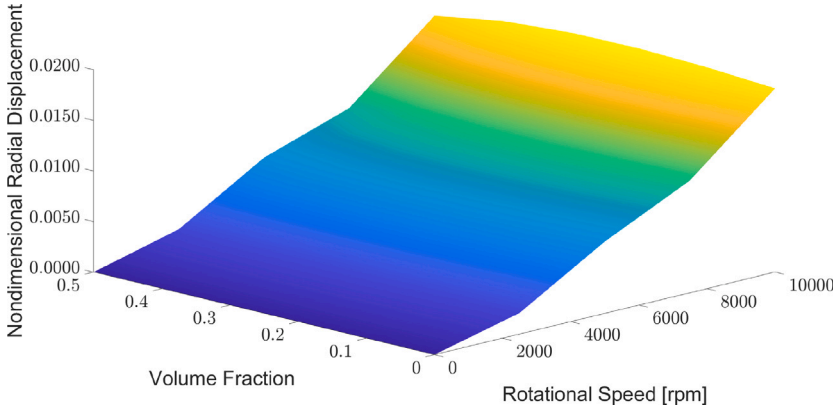

Fig. 12. Nondimensional radial displacement versus rotational speed and volume fraction.

4.2.2. Modal analysis

Performing the modal analysis, the first eight modes are investigated. The surface plots of the first three natural frequencies are shown in Fig. 13. Furthermore, the calculated first eight natural frequencies and the corresponding mode shapes are presented in Table 6 and Fig. 14.

Analysing the prestressed modal behaviour, it is evident that an increase in rotational speed and volume fraction does influence the resonant frequency. This statement is supported by the alterations observed in the 1st through the 8th natural frequencies.

Specifically, at a constant volume fraction, a rise in rotational speed causes an increase in the natural frequencies due to the typical stiffening effects of the loads. For instance, when the alloy (not the foams) is used to manufacture the blade, the 1st mode frequency displays an increase of 34% as the rotational speed goes from 0 to 104 rad/s.

Moreover, at a fixed rotational speed, an elevation in the volume fractionV_f also leads to decreasing natural frequencies. Remembering the observation from the static simulations, the drop in mass is noted as more significant compared to the fall in stiffness. On the other hand, these declining natural frequencies suggest the exact opposite of what is seen in the static analyses. Here, the reduction in the stiffness properties seems to be more significant than the drop in the inertial properties. For example, when the blade is stationary, the 1st mode frequency decreases by 19% as V_f goes from 0 to 0.5.

Furthermore, an overall inspection of the frequency changes across the different modes reveals a consistent trend. The natural frequencies decrease when the volume fraction increases. In contrast, the natural

Table 5
Nondimensionalised results of the static analysis.

Volume fraction (V_f)	Rotational speed [rad/s]	Maximum von Mises stress	Maximum principal stress	Maximum displacement	Maximum radial displacement
0	26	2.44×10^{-4}	2.81×10^{-4}	7.46×10^{-3}	2.08×10^{-3}
0.1	26	2.14×10^{-4}	2.46×10^{-4}	7.82×10^{-3}	2.20×10^{-3}
0.2	26	1.83×10^{-4}	2.10×10^{-4}	8.01×10^{-3}	2.30×10^{-3}
0.3	26	1.53×10^{-4}	1.53×10^{-4}	7.99×10^{-3}	2.34×10^{-3}
0.4	26	1.34×10^{-4}	1.40×10^{-4}	7.64×10^{-3}	2.32×10^{-3}
0.5	26	1.43×10^{-4}	1.44×10^{-4}	6.79×10^{-3}	2.19×10^{-3}
0	52	8.70×10^{-4}	9.95×10^{-4}	2.55×10^{-2}	7.10×10^{-3}
0.1	52	7.55×10^{-4}	8.65×10^{-4}	2.64×10^{-2}	7.44×10^{-3}
0.2	52	6.40×10^{-4}	7.35×10^{-4}	2.67×10^{-2}	7.68×10^{-3}
0.3	52	5.95×10^{-4}	6.10×10^{-4}	2.64×10^{-2}	7.77×10^{-3}
0.4	52	6.05×10^{-4}	6.10×10^{-4}	2.49×10^{-2}	7.66×10^{-3}
0.5	52	6.15×10^{-4}	6.15×10^{-4}	2.19×10^{-2}	7.23×10^{-3}
0	78	1.46×10^{-3}	1.63×10^{-3}	3.89×10^{-2}	1.11×10^{-2}
0.1	78	1.47×10^{-3}	1.47×10^{-3}	3.93×10^{-2}	1.15×10^{-2}
0.2	78	1.47×10^{-3}	1.47×10^{-3}	3.88×10^{-2}	1.16×10^{-2}
0.3	78	1.45×10^{-3}	1.46×10^{-3}	3.69×10^{-2}	1.16×10^{-2}
0.4	78	1.44×10^{-3}	1.44×10^{-3}	3.33×10^{-2}	1.11×10^{-2}
0.5	78	1.40×10^{-3}	1.41×10^{-3}	2.71×10^{-2}	1.01×10^{-2}
0	104	3.28×10^{-3}	3.29×10^{-3}	6.43×10^{-2}	1.82×10^{-2}
0.1	104	3.19×10^{-3}	3.20×10^{-3}	6.45×10^{-2}	1.86×10^{-2}
0.2	104	3.07×10^{-3}	3.08×10^{-3}	6.35×10^{-2}	1.90×10^{-2}
0.3	104	2.89×10^{-3}	2.90×10^{-3}	5.97×10^{-2}	1.91×10^{-2}
0.4	104	2.77×10^{-3}	2.78×10^{-3}	5.58×10^{-2}	1.83×10^{-2}
0.5	104	2.60×10^{-3}	2.61×10^{-3}	4.78×10^{-2}	1.72×10^{-2}

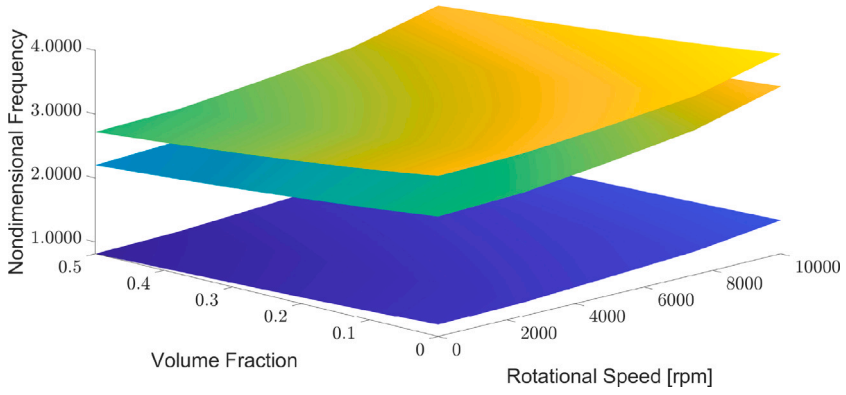

Fig. 13. Nondimensional frequency versus rotational speed and volume fraction for the first three modes.

frequencies rise as the rotational speed increases. This pattern holds across all eight natural frequencies. Since the physical phenomena that cause these two trends are not mode-dependent. The reduction of the stiffness and inertial properties and the stiffening effects of the loads influence the system as a whole and not some particular mode.

It is worth mentioning that the impact of rotational speed on the natural frequencies seems to be greater than the volume fraction's influence. This difference becomes more apparent at higher rotational speeds and modes. Therefore, the rotational speed's role in affecting the system's dynamics may be considered more substantial, necessitating careful checks and adjustments during the design process as well as the operation.

Finally, the results reveal that the dynamics of the blade have a complex nature. The parameters that affect the results of the static analysis are shown to cause different tendencies when it comes to the modal analysis of the blade. Therefore, the dynamics of the blade need to be a completely separate parameter for the design when employing foams to manufacture the fan blade.

Finally, the results of the modal analyses presented in this study are in good agreement regarding the physics and tendencies/trends compared to the studies in the literature that incorporates a foam cor for blade applications [26,27].

5. Conclusions

This study presents a numerical investigation of the mechanical properties of Ti-6Al-4V alloy foams and their applicability in the design of aero-engine fan blades. Taking advantage of the Mori–Tanaka mean-field homogenisation and FE methods, the effects of the volume fraction of voids on the foam's mechanical characteristics are assessed. Also, using the FE method, a numerical model of a representative fan blade is constructed incorporating these calculated material properties. This numerical model is used to execute static and modal analyses of a fan blade made of foams under its representative operating conditions. Through these processes, the study outlines the key trade-offs to consider when applying this material in fan blade design, emphasising the importance of carefully balancing these aspects in the materials selection and design process.

The results of the Mori–Tanaka and the FE analysis indicate that as the volume fraction of voids in the foam increases, Young's modulus

Table 6
Nondimensionalised natural frequencies calculated through the modal analysis.

Volume fraction (V_f)	Rotational speed [rad/s]	1st mode [Hz]	2nd mode [Hz]	3rd mode [Hz]	4th mode [Hz]	5th mode [Hz]	6th mode [Hz]	7th mode [Hz]	8th mode [Hz]
0	0	1.00	2.70	3.33	11.38	13.60	20.29	24.16	30.25
0.1	0	0.95	2.57	3.18	10.84	12.97	19.34	23.03	28.84
0.2	0	0.91	2.46	3.04	10.38	12.41	18.52	22.05	27.61
0.3	0	0.88	2.37	2.92	9.98	11.93	17.79	21.18	26.52
0.4	0	0.84	2.28	2.82	9.61	11.49	17.14	20.41	25.56
0.5	0	0.81	2.20	2.72	9.29	11.10	16.56	19.72	24.69
0	26	1.03	2.75	3.37	11.39	13.80	20.38	24.17	30.22
0.1	26	0.98	2.63	3.21	10.86	13.17	19.43	23.04	28.81
0.2	26	0.94	2.52	3.08	10.41	12.62	18.61	22.06	27.58
0.3	26	0.91	2.43	2.96	10.00	12.14	17.89	21.20	26.50
0.4	26	0.88	2.34	2.86	9.65	11.70	17.25	20.43	25.55
0.5	26	0.85	2.27	2.77	9.33	11.31	16.67	19.75	24.70
0	52	1.10	2.90	3.47	11.45	14.34	20.63	24.20	30.15
0.1	52	1.06	2.78	3.33	10.93	13.72	19.70	23.08	28.76
0.2	52	1.02	2.69	3.20	10.49	13.18	18.89	22.11	27.55
0.3	52	0.99	2.60	3.09	10.10	12.69	18.18	21.26	26.49
0.4	52	0.96	2.52	2.99	9.77	12.25	17.54	20.51	25.56
0.5	52	0.93	2.46	2.90	9.47	11.85	16.97	19.83	24.75
0	78	1.18	3.08	3.62	11.57	14.86	20.92	24.27	30.17
0.1	78	1.14	2.97	3.48	11.07	14.25	20.00	23.16	28.80
0.2	78	1.10	2.88	3.35	10.65	13.70	19.20	22.20	27.62
0.3	78	1.07	2.81	3.25	10.28	13.21	18.49	21.36	26.59
0.4	78	1.04	2.74	3.15	9.97	12.76	17.86	20.61	25.71
0.5	78	1.01	2.68	3.07	9.70	12.32	17.29	19.95	24.95
0	104	1.34	3.44	3.95	11.85	15.87	21.52	24.41	30.22
0.1	104	1.30	3.34	3.82	11.37	15.26	20.61	23.31	28.89
0.2	104	1.27	3.27	3.70	10.98	14.71	19.82	22.35	27.74
0.3	104	1.24	3.20	3.59	10.64	14.21	19.12	21.52	26.76
0.4	104	1.22	3.15	3.49	10.35	13.74	18.49	20.78	25.92
0.5	104	1.19	3.11	3.40	10.12	13.30	17.92	20.13	25.21

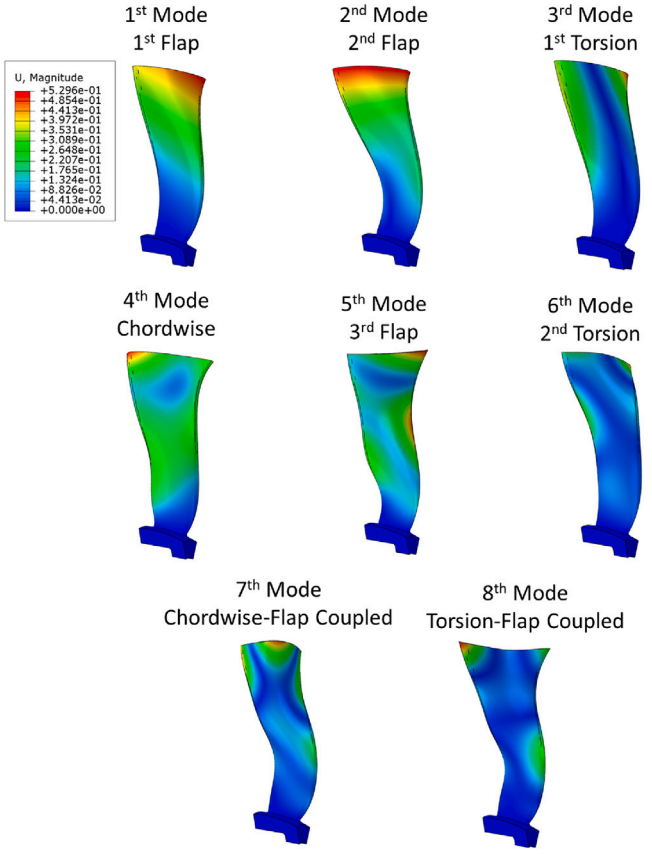

Fig. 14. The first eight mode shapes of the fan blade model.

and specific modulus decrease. This trend suggests that whilst the material becomes lighter with a higher volume fraction of voids, its capacity to resist deformations reduces, indicating the inherent trade-offs to be considered in the design and materials selection process.

Static simulations of the fan blade reveal that as the volume fraction of voids increases, the maximum von Mises stress and maximum principal stress decrease, which can be primarily attributed to the reduction in rotational body forces. Maximum displacement and radial displacement initially increase with the volume fraction of voids, reaching a peak, and then decline at higher rotational speeds.

Besides, the modal analysis provides a different side of the mechanics of the blade, illustrating a different correlation between the volume fraction and the natural frequencies, suggesting that the dynamics of the blade change when foams are employed. The rotational speed is found to have a more substantial impact on the natural frequencies, underscoring the need for careful considerations during design and operations.

This study lays a groundwork for future research that can explore this topic further. Whilst the present work provides a clear overview of the potential use of Ti-6Al-4V alloy foams in aero-engine fan blades, it highlights some complexities in the impact of various parameters. However, there are more parameters to consider, which is essential to gain a sufficient understanding to be able to achieve a complete design. Among these parameters, more comprehensive loading conditions in the numerical models can be considered. These loading conditions should include thermal loads and steady-state dynamic loads as well as transient dynamic loads. The forced response of these blades made of foam needs to be performed, as well as cases like bird strike are necessary, which requires elastoplastic material modelling.

Declaration of competing interest

The authors declare that they have no known competing financial interests or personal relationships that could have appeared to influence the work reported in this paper.

Data availability

No data was used for the research described in the article.

Acknowledgement

Mertol Tüfekci would like to acknowledge computational resources and support provided by the Imperial College Research Computing Service (http://doi.org/10.14469/hpc/2232).

References

[1] R.H. Mao, S.A. Meguid, T.Y. Ng, Transient three dimensional finite element analysis of a bird striking a fan blade, Int. J. Mech. Mater. Des. 4 (2008) 79–96, http://dx.doi.org/10.1007/s10999-008-9067-1.

[2] R.H. Mao, S.A. Meguid, T.Y. Ng, Finite element modeling of a bird striking an engine fan blade, J. Aircr. 44 (2007) 583–596, http://dx.doi.org/10.2514/1.24568.

[3] L.M. Amoo, On the design and structural analysis of jet engine fan blade structures, Prog. Aerosp. Sci. 60 (2013) 1–11, http://dx.doi.org/10.1016/j.paerosci.2012.08.002.

[4] M. Tufekci, Q. Rendu, J. Yuan, J.P. Dear, L. Salles, A.V. Cherednichenko, Stress and modal analysis of a rotating blade and the effects of nonlocality, in: Proceedings of the ASME Turbo Expo, Vol. 10B-2020, American Society of Mechanical Engineers, 2020, pp. 1–12, http://dx.doi.org/10.1115/GT2020-14821, https://asmedigitalcollection.asme.org/GT/proceedings/GT2020/84225/Virtual,Online/1095287.

[5] H. Koç, Ö.E. Genel, M. Tüfekci, E. Tüfekci, Analysis of the dynamical behaviour of spinning annular disks with various boundary conditions, Mech. Based Des. Struct. Mach. (2021) 1–25, http://dx.doi.org/10.1080/15397734.2021.1999269, URL: https://www.tandfonline.com/doi/full/10.1080/15397734.2021.1999269.

[6] M. Tufekci, O.E. Genel, H. Koc, O. Oldac, E. Tufekci, Vibrations of a rotating disk under perpendicular spacefixed forces, Gazi Univ. J. Sci. 32 (2019) 273–284.

[7] C. Chahine, T. Verstraete, L. He, Multidisciplinary design optimization of an aero-engine fan blade with consideration of bypass and core performance, 2015, pp. 5–10.

[8] R.M. Coroneos, R.S.R. Gorla, Structural analysis and optimization of a composite fan blade for future aircraft engine, Int. J. Turbo Jet Engines 29 (2012) 131–164, http://dx.doi.org/10.1515/tjj-2012-0024.

[9] A.E. Albanesi, I. Peralta, F. Bre, B.A. Storti, V.D. Fachinotti, An optimization method based on the evolutionary and topology approaches to reduce the mass of composite wind turbine blades, Struct. Multidiscip. Optim. 62 (2020) 619–643, http://dx.doi.org/10.1007/s00158-020-02518-2.

[10] P. Dhopade, A.J. Neely, Aeromechanical modeling of rotating fan blades to investigate high-cycle and low-cycle fatigue interaction, J. Eng. Gas Turb. Power 137 (2015) http://dx.doi.org/10.1115/1.4028717.

[11] B.M. Santhosh, M. Tufekci, L. Salles, F. Scarpa, J. Yuan, Flutter mitigation of turbofan blades using viscoelastic patches, 2022.

[12] J.G. Marshall, M. Imregun, An analysis of the aeroelastic behaviour of a typical fan-blade with emphasis on the flutter mechanism, in: ASME 1996 International Gas Turbine and Aeroengine Congress and Exhibition, GT 1996, Vol. 5, 1996, http://dx.doi.org/10.1115/96-GT-078.

[13] Q. Rendu, L. Salles, Development of a surrogate model for uncertainty quantification of compressor performance due to manufacturing tolerance, J. Global Power Propuls. Soc. 7 (2023) 257–268, http://dx.doi.org/10.33737/jgpps/168293, URL: https://journal.gpps.global/Development-of-a-surrogate-model-for-uncertainty-quantification-of-compressor-performance,168293,0,2.html.

[14] M. Tüfekci, Ö.E. Genel, A. Tatar, E. Tüfekci, Dynamic analysis of composite wind turbine blades as beams: An analytical and numerical study, Vibration 4 (2020) 1–15, http://dx.doi.org/10.3390/vibration4010001, URL: https://www.mdpi.com/2571-631X/4/1/1.

[15] M. Tüfekci, B. Özkal, C. Maharaj, H. Liu, J.P. Dear, L. Salles, Strain-rate-dependent mechanics and impact performance of epoxy-based nanocomposites, Compos. Sci. Technol. 233 (2023) 109870, http://dx.doi.org/10.1016/j.compscitech.2022.109870, URL: https://linkinghub.elsevier.com/retrieve/pii/S0266353822006121.

[16] J. Min, K. Duffy, B. Choi, A. Provenza, N. Kray, American Institute of Aeronautics and Astronautics, Reston, Virigina, 2012, http://dx.doi.org/10.2514/6.2012-1644, URL: http://arc.aiaa.org/doi/abs/10.2514/6.2012-1644.

[17] J. Xiao, Y. Chen, Q. Zhu, J. Lee, T. Ma, A general ply design for aero engine composite fan blade, in: Proceedings of the ASME Turbo Expo, Vol. 7A-2017, 2017, pp. 1–8, http://dx.doi.org/10.1115/GT201764377.

[18] G.J. Davies, S. Zhen, Metallic foams: their production, properties and applications, J. Mater. Sci. 18 (1983) 1899–1911, http://dx.doi.org/10.1007/BF00554981.

[19] L.J. Gibson, Mechanical behavior of metallic foams, Annu. Rev. Mater. Sci. 30 (2000) 191–227, http://dx.doi.org/10.1146/annurev.matsci.30.1.191.

[20] P.R. Marur, Numerical estimation of effective elastic moduli of syntactic foams, Finite Elem. Anal. Des. 46 (2010) 1001–1007, http://dx.doi.org/10.1016/j.finel.2010.07.006.

[21] F.V. Antunes, J.A. Ferreira, C. Capela, Numerical modelling of the Young's modulus of syntactic foams, Finite Elem. Anal. Des. 47 (2011) 78–84, http://dx.doi.org/10.1016/j.finel.2010.09.007.

[22] T. Chen, G.J. Dvorak, Y. Benveniste, Mori-tanaka estimates of the overall elastic moduli of certain composite materials, J. Appl. Mech. Trans. ASME 59 (1992) 539–546, http://dx.doi.org/10.1115/1.2893757.

[23] P. Jadhav, Innovative designs of embedded foam inserts in aerospace composite structures, Mater. Today: Proc. 21 (2020) 1164–1168, http://dx.doi.org/10.1016/j.matpr.2020.01.066, URL: https://linkinghub.elsevier.com/retrieve/pii/S2214785320301279.

[24] S.V. Raj, L.J. Ghosn, Failure maps for rectangular 17-4PH stainless steel sandwiched foam panels, Mater. Sci. Eng. A 474 (2008) 88–95, http://dx.doi.org/10.1016/j.msea.2007.03.102.

[25] B. Castanie, C. Bouvet, M. Ginot, Review of composite sandwich structure in aeronautic applications, Composites C 1 (2020) 100004, http://dx.doi.org/10.1016/j.jcomc.2020.100004.

[26] J.B. Min, L.J. Ghosn, B.A. Lerch, A study for stainless steel fan blade design with metal foam core, J. Sandw. Struct. Mater. 17 (2015) 56–73, http://dx.doi.org/10.1177/1099636214554181.

[27] J.B. Min, L.J. Ghosn, B.A. Lerch, S.V. Raj, F.A. Holland, M.G. Hebsur, Analysis of Stainless Steel Sandwich Panels with a Metal Foam Core for Lightweight Fan Blade Design, Vol. 5, 2004, pp. 3486–3495, http://dx.doi.org/10.2514/6.2004-1836.

[28] S. Hilgenfeldt, A. Kraynik, D. Reinelt, J. Sullivan, Bubble shapes in foams: The importance of being isotropic, in: APS March Meeting Abstracts, in: APS Meeting Abstracts, vol. 2004, 2004, H21.008.

[29] L.J. Gibson, M.F. Ashby, The mechanics of three-dimensional cellular materials, Proc. R. Soc. Lond. Ser. A Math. Phys. Eng. Sci. 382 (1982) 43–59, http://dx.doi.org/10.1098/rspa.1982.0088, URL: https://royalsocietypublishing.org/doi/10.1098/rspa.1982.0088.

[30] A.P. Roberts, E.J. Garboczi, Computation of the linear elastic properties of random porous materials with a wide variety of microstructure, Proc. R. Soc. Lond. Ser. A Math. Phys. Eng. Sci. 458 (2002) 1033–1054, http://dx.doi.org/10.1098/rspa.2001.0900.

[31] L. Liu, Z. Huang, A note on mori-tanaka's method, Acta Mech. Solida Sin. 27 (2014) 234–244, http://dx.doi.org/10.1016/S0894-9166(14)60033-1.

[32] T. Mori, K. Tanaka, Average stress in matrix and average elastic energy of materials with misfitting inclusions, Acta Metall. 21 (1973) 571–574, http://dx.doi.org/10.1016/0001-6160(73)90064-3.

[33] A. Pontefisso, M. Zappalorto, M. Quaresimin, An efficient RVE formulation for the analysis of the elastic properties of spherical nanoparticle reinforced polymers, Comput. Mater. Sci. 96 (2015) 319–326, http://dx.doi.org/10.1016/j.commatsci.2014.09.030.

[34] I.V. Singh, A.S. Shedbale, B.K. Mishra, Material property evaluation of particle reinforced composites using finite element approach, J. Compos. Mater. 50 (2016) 2757–2771, http://dx.doi.org/10.1177/0021998315612539.

[35] R.V. Pucha, J. Worthy, Representative volume element-based design and analysis tools for composite materials with nanofillers, J. Compos. Mater. 48 (2014) 2117–2129, http://dx.doi.org/10.1177/0021998313494916.

[36] J.D. Fidelus, E. Wiesel, F.H. Gojny, K. Schulte, H.D. Wagner, Thermo-mechanical properties of randomly oriented carbon/epoxy nanocomposites, Composites A 36 (2005) 1555–1561, http://dx.doi.org/10.1016/j.compositesa.2005.02.006.

[37] C. Aguilar, C. Salvo, J. Henriquez, D. Vega, I. Alonso, L. Muñoz, Computational analysis of the graded porosity distribution on the elastic modulus of Ti foams, Mater. Today Commun. 35 (2023) http://dx.doi.org/10.1016/j.mtcomm.2023.106391.

[38] H. Choi, H. Park, J.H. Um, W.S. Yoon, H. Choe, Processing and characterization of titanium dioxide grown on titanium foam for potential use as Li-ion electrode, Appl. Surf. Sci. 411 (2017) 363–367, http://dx.doi.org/10.1016/j.apsusc.2017.03.122.

[39] Z. Esen, Ş. Bor, Characterization of Ti-6Al-4V alloy foams synthesized by space holder technique, Mater. Sci. Eng. A 528 (2011) 3200–3209, http://dx.doi.org/10.1016/j.msea.2011.01.008.

[40] I.M. Gitman, H. Askes, L.J. Sluys, Representative volume: Existence and size determination, Eng. Fract. Mech. 74 (2007) 2518–2534, http://dx.doi.org/10.1016/j.engfracmech.2006.12.021.

[41] G. Catalanotti, On the generation of RVE-based models of composites reinforced with long fibres or spherical particles, Compos. Struct. 138 (2016) 84–95, http://dx.doi.org/10.1016/j.compstruct.2015.11.039.

[42] D.P. Mandal, D.D. Majumdar, R.K. Bharti, J.D. Majumdar, Microstructural characterisation and property evaluation of titanium cenosphere syntactic foam developed by powder metallurgy route, Powder Metall. 58 (2015) 289–299, http://dx.doi.org/10.1179/1743290115Y.0000000012.

[43] İ. Pir, M. Tüfekci, E. Tüfekci, The mechanics of 3-dimensional elastic foams investigation of transverse vibrations of circular annular thin plates view project analytical solutions of static and dynamic problems of curved nanobeams view project, 2022, URL: https://www.researchgate.net/publication/361492403.

[44] M. Tüfekci, I. Pir, E. Tüfekci, Nondimensional analysis of two-dimensional elastic porous materials with regularly distributed circular holes, 2021.

[45] Y. Huang, A.J. Kinloch, Modelling of the toughening mechanisms in rubber-modified epoxy polymers - part I finite element analysis studies, J. Mater. Sci. 27 (10) (1992) 2753–2762, http://dx.doi.org/10.1007/BF00540702, URL: http://www.springerlink.com/index/10.1007/BF00540702.

[46] L. Pérez, S. Lascano, C. Aguilar, D. Domancic, I. Alfonso, Simplified fractal FEA model for the estimation of the Young's modulus of ti foams obtained by powder metallurgy, Mater. Des. 83 (2015) 276–283, http://dx.doi.org/10.1016/j.matdes.2015.06.038.